Tellus (1990), *42A*, 328–342

The importance of non-quasigeostrophic forcing during the development of a blocking anticyclone

By CHIH-HUA TSOU and PHILLIP J. SMITH, *Department of Earth and Atmospheric Sciences, Purdue University, West Lafayette, IN 47907, USA*

(Manuscript received 28 March 1989; in final form 11 July 1989)

ABSTRACT

Non-quasigeostrophic (NQG) processes present prior to and during the development of a blocking anticyclone over the southern tip of Greenland on 21 January 1979 are diagnosed by comparing energy quantities and height tendencies determined from quasigeostrophic (QG) estimates with the same quantities obtained from more general formulations. Calculations were done using GLA FGGE Level III-b analyses on a 4° lat by 5° long grid. Energetics results indicate that NQG processes strengthened the intensity of the block and a precursor explosive cyclone and that a portion of this increase resulted from enhanced baroclinic conversion of eddy potential to eddy kinetic energy and reduced barotropic energy conversion from eddy to zonal flow. The height tendency fields show that the QG calculations, which generally yielded height changes that were larger than the more general height tendency model, produced smaller height changes associated with the northward amplification of the ridge from which the block ultimately formed. Further, these smaller values were primarily due to the QG vorticity advection. This suggests that NQG vorticity advection, which usually acted to moderate the wave developments, enhanced the block development. In fact, it is suggested that QG forcing might not have been adequate to produce the observed block development. Non-quasigeostrophic processes were also significant in the static stability advection term but were of little consequence in the differential thermal advection.

1. Introduction

A feature of the large-scale circulation that has attracted much attention in recent years is the blocking anticyclone. Because of their large scale and relatively low Rossby number, such events are often studied using a quasigeostrophic approach. However, Bengtsson (1981), who investigated the predictability of blocking using a series of numerical models, found that high resolution primitive equation models successfully predicted a blocking event in great detail, while a quasigeostrophic model was inadequate for such predictions. This suggests that non-quasigeostrophic processes might play an important role during large-scale blocking.

Other studies also support this supposition. Appearing most prominently are the several studies (e.g., Green, 1977; Hansen and Chen, 1982; Colucci, 1985, 1987; Mullen, 1987; and Tsou and Smith, 1990) that have shown that synoptic-scale cyclones, which may have significant non-quasigeostrophic features, often precede and have important impacts on the evolution of blocking highs. Further, Gall (1977) found that non-quasigeostrophic effects produce significant asymmetries in a baroclinic wave even when the Rossby number is small. These asymmetries result in significant differences between the eddy fluxes in primitive equation and quasigeostrophic models, especially in the eddy horizontal momentum flux. However, using quasigeostrophic and primitive equation dynamics to diagnose the effects of cyclone waves on the large-scale flow, Mudrick (1982) found that the zonally and time-averaged eddy heat fluxes from the two were similar. Hence, even when non-quasigeostrophic processes are important, the importance may not

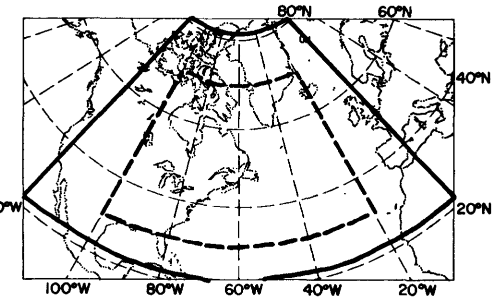

Fig. 1. Geographic location of the horizontal computational domain (area inside the heavy solid line) and the area average box for energy quantities (area inside the heavy dashed line).

extend to all features of a wave system's development.

The objective of this study is to examine whether non-quasigeostrophic processes are important during the development of a blocking anticyclone that appeared over the southern tip of Greenland on 21 January 1979 and was preceded by an upstream cyclone that developed rapidly between 18 and 19 January. This is an extension of work recently reported by Tsou and Smith (1989), hereafter referred to as TS. In order to diagnose the total wave system in which the block and upstream cyclone were contained, the eddy kinetic energy content and baroclinic and barotropic energy exchanges are examined using both analyzed (AN) and quasigeostrophic (QG) fields. To examine the more detailed dynamics of the block development, both QG (Holton, 1979) and extended (EXT, Tsou et al., 1987) height tendency equations are used. Non-quasigeostrophic (NQG) influences are inferred by comparing QG diagnoses of the energy and tendency quantities with those derived from the more general form of the respective quantities.

2. Methodology

2.1. Energetics

The eddy kinetic energy content can be defined as

$$\mathrm{KE}=\frac{1}{g}\int_{p_t}^{p_s}\left[\overline{\frac{\boldsymbol{V}'\cdot\boldsymbol{V}'}{2}}\right]\mathrm{d}p=\frac{1}{g}\int_{p_t}^{p_s}[\overline{k'}]\,\mathrm{d}p, \tag{1}$$

where k' is the horizontal eddy kinetic energy per unit mass $[\frac{1}{2}(u'^2+v'^2)$, $u=$ west–east wind component, $v=$ south–north wind component]; and $\boldsymbol{V}$ is the horizontal wind vector. The overbar corresponds to a zonal average along each latitude over the interior domain in Fig. 1; the bracket is the averaging operator in the y-direction; the prime represents the departure of a given point from its zonal mean; and the subscripts s and t refer to the surface and top (100 mb) pressure levels, respectively.

Following Robertson and Smith (1983), the eddy kinetic energy equation for a limited domain can be expressed as

$$\frac{\partial \mathrm{KE}}{\partial t}=-\frac{1}{g}\int_{p_t}^{p_s}[\overline{\omega'\alpha'}]\,\mathrm{d}p$$
(A)

$$-\frac{1}{g}\int_{p_t}^{p_s}[\overline{\boldsymbol{V}'\cdot(\boldsymbol{V}'\cdot\nabla)\overline{\boldsymbol{V}}}]\,\mathrm{d}p$$
(B)

$$-\frac{1}{g}\int_{p_t}^{p_s}\left[\overline{\boldsymbol{V}'\cdot\omega'\frac{\partial\overline{\boldsymbol{V}}}{\partial p}}\right]\mathrm{d}p-\frac{1}{g}\int_{p_t}^{p_s}[\overline{\nabla\cdot k'\boldsymbol{V}}]\,\mathrm{d}p$$
(C) (D)

$$-\frac{1}{g}\int_{p_t}^{p_s}\left[\overline{\frac{\partial k'\omega}{\partial p}}\right]\mathrm{d}p-\frac{1}{g}\int_{p_t}^{p_s}[\overline{\nabla\cdot\Phi'\boldsymbol{V}'}]\,\mathrm{d}p$$
(E) (F)

$$-\frac{1}{g}\int_{p_t}^{p_s}\left[\overline{\frac{\partial\Phi'\omega'}{\partial p}}\right]\mathrm{d}p+\frac{1}{g}\int_{p_t}^{p_s}[\overline{\boldsymbol{V}'\cdot\boldsymbol{F}'}]\,\mathrm{d}p$$
(G) (H)

$$+\frac{1}{g}\int_{p_t}^{p_s}\left[\overline{\frac{\boldsymbol{V}_s'\cdot\boldsymbol{V}_s'}{2}\frac{\partial p_s}{\partial t}}\right], \tag{2}$$
(I)

where Φ is the geopotential, ω the vertical motion in isobaric coordinates, ∇ the horizontal del operator on an isobaric surface, α the specific volume, and $\boldsymbol{F}$ the frictional force. Term (A), identified by Robertson and Smith as the release of eddy available potential energy, is used here to represent the baroclinic exchange between available potential and kinetic energy (CE); (B) and (C) are the horizontal and vertical components of the barotropic exchange between eddy and zonal kinetic energy (CK), (D) and (E) are the horizontal and vertical transports of k', (F) and (G) are the horizontal and vertical boundary work, (H) is the frictional dissipation, and (I) is the KE change occurring because of the time variation of mass within the volume being considered. The energy quantities considered in this study are KE, CE, and CK. These quantities have the same expression in both their AN and QG forms. However, the analyzed horizontal and vertical motion components used in the AN form are replaced by their quasigeostrophic counterparts in the QG form. The ω used for the energy and height tendency calculations described later are solved from either the quasigeostrophic (Holton, 1979) or extended (TS) form of the omega equation.

2.2. Height tendencies

Height tendency equations were chosen to diagnose the dynamics of the block development because height tendencies are easily related to wave development and propagation and because the influence of different forcing processes on the total height change can be diagnosed conveniently. As specified in Tsou et al. (1987), the EXT and QG height tendency equations can be expressed, respectively, as

$$\left[\nabla^2 + \frac{(\zeta+f)f}{\sigma}\frac{\partial}{\partial p^2}\right]\frac{\partial \Phi}{\partial t} = \underset{\text{(A)}}{-fV\cdot\nabla(\zeta+f)} + \underset{\text{(B)}}{\frac{(\zeta+f)fR}{\sigma}\frac{\partial}{\partial p}\left(V\cdot\nabla\frac{T}{p}\right)} - \underset{\text{(C)}}{\frac{(\zeta+f)f}{\sigma}\omega\frac{\partial\sigma}{\partial p}} - \underset{\text{(D)}}{\frac{(\zeta+f)fR}{\sigma}\frac{\partial}{c_p\,\partial p}\left(\frac{\dot{q}}{p}\right)} \tag{3}$$

and

$$\left[\nabla^2 + \frac{f_0^2}{\sigma_g}\frac{\partial}{\partial p^2}\right]\frac{\partial \Phi}{\partial t} = \underset{\text{(A)}}{-f_0 V_g\cdot\nabla(\zeta_g+f)} + \underset{\text{(B)}}{\frac{f_0^2}{\sigma_g}\frac{\partial}{\partial p}\left(-V_g\cdot\nabla\frac{T}{p}\right)} - \underset{\text{(C)}}{\frac{f_0^2}{\sigma_g}\omega_g\frac{\partial\sigma_g}{\partial p}}, \tag{4}$$

where $\sigma = -RT/p\theta\ (\partial\theta/\partial p)$ is the static stability parameter; ζ the vertical component of relative vorticity; f the coriolis parameter; $\dot{q}$ the diabatic heating rate; T the temperature; θ the potential temperature; c_p the specific heat of dry air at constant pressure; and R the dry air constant. In (4), subscript g refers to QG quantities; σ_g is a function of pressure only; f_0 is a constant coriolis parameter; and V_g and ζ_g are defined as $(k \wedge \nabla\Phi)/f_0$ and $(\nabla^2\Phi)/f_0$, respectively. Height z enters (3) and (4) through $\Phi = gz$, where $g = 9.8\ \mathrm{m\ s^{-2}}$. A discussion of the physical meaning of the terms can be found in Tsou et al. (1987) and Smith and Tsou (1988). It will suffice here to note that terms (A), (B), (C), and (D) represent the forcing due to horizontal vorticity advection (VORT), differential horizontal temperature advection (THER), differential diabatic heating (HEAT), and vertical advection of static stability (STAB). Note that term (D) is omitted from (4) because only small $\dot{q}$ values are permitted in QG theory (Phillips, 1963). Since small $\dot{q}$ would contribute little to the sizeable QG tendencies found in this study, QG heating calculations were omitted. Also, the QG form usually omits term (C) for simplicity (see Holton (1979) p. 131). However, results presented later show this term to be equally significant to terms (A) and (B) in both (3) and (4).

Clearly, (3) and (4) are quite similar. However, (3) replaces the QG wind, vertical motion, and relative vorticity with their analyzed values; allows three-dimensionally varying σ; and permits strong diabatic heating. The NQG implications of the first two of the properties will be revealed by comparing the AN and QG forms of terms (A), (B), and (C). In principle the impact of strong diabatic heating would be seen in term (D). However, calculations have shown this term to have little influence on the block. Therefore, it is not included in later discussions.

Height tendencies were solved using successive overrelaxation with zero tendencies as lateral boundary conditions and zero vertical derivatives of height tendency as upper and lower boundary conditions. More detailed descriptions of the computational procedures can be found in TS. For simplicity, height tendency results are generally restricted to 500 mb, primarily because the block development is well depicted at this level and because calculations at 700 and 300 mb

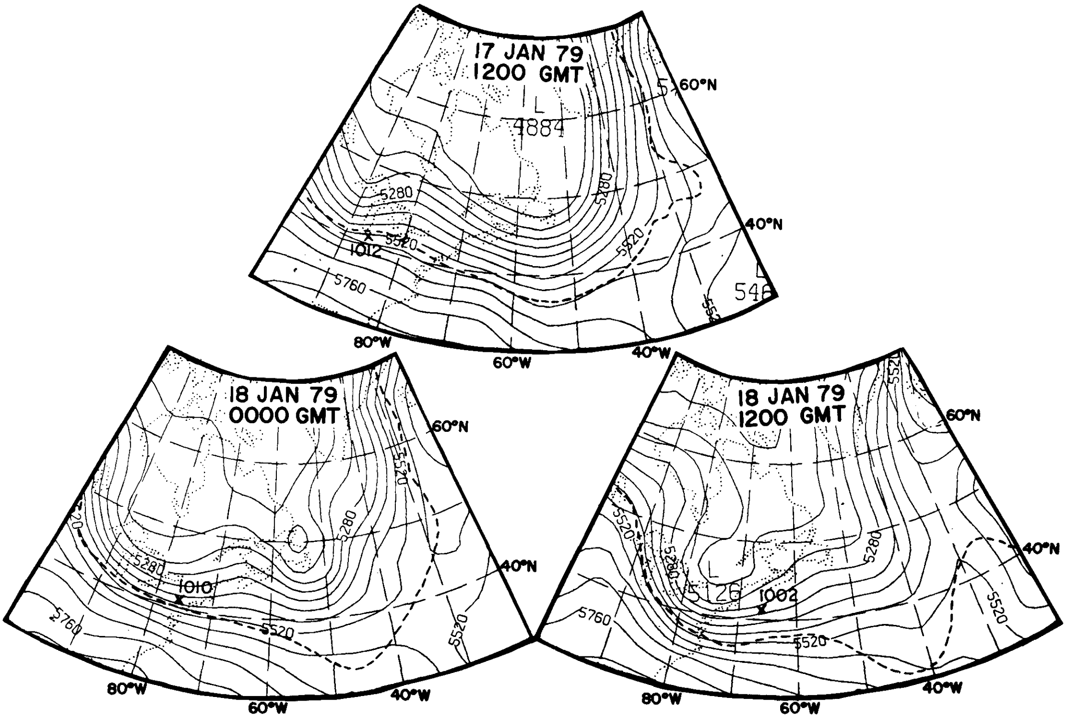

Fig. 2. 500 mb heights (solid, *m*, $\Delta Z = 60$ m) and 250 K isotherm (dashed) for 12.00 GMT 17 January through 12.00 GMT 18 January 1979. "X" represents the location of the surface cyclone with central sea level pressure indicated in mb.

suggest that the 500 mb results are representative of the middle and upper troposphere.

3. Data and synoptic discussion

SOP-I FGGE III-b analyses at mandatory levels obtained from the Goddard Laboratory for Atmospheres (GLA) were used for this study. The objective analysis procedure developed at GLA is a successive correction method of the Cressman (1959) type, but modified to include variable data density and quality. The assimilation/forecast model utilized for data analysis is the global fourth-order version of the GLA General Circulation Model. To focus on the Atlantic block and its upstream cyclone, only a portion of the original global data set, covering a domain from 0° to 120°W and 22° to 82°N (Fig. 1) during the period 17–21 January 1979, was selected for analysis in this study. In addition, the mandatory level data (4° latitude by 5° longitude) were interpolated or extrapolated to standard isobaric surfaces from 1050 mb to 50 mb in 50 mb increments. The vertical interpolation technique used was the same as described in Baker (1983) in order to be consistent with the original data manipulation. More detailed discussions of the data and analysis procedures can be found in Baker (1983).

Figs. 2 and 3 show the time evolution of the 500 mb height field and 250°K isotherm and the location of an associated surface cyclone that originated over Lake Michigan at 12.00 GMT 17 January. In the initial 24-h period, a short-wave ridge downstream from the surface cyclone propagated eastward without significantly changing its amplitude. However, as the cyclone center passed the New England shore between 00.00 and 12.00 GMT 18 January, both the short wave ridge and surface cyclone intensified and reduced their propagation speed. The sea level pressure of the latter then dramatically decreased from 1002 mb to 971 mb, reaching a minimum

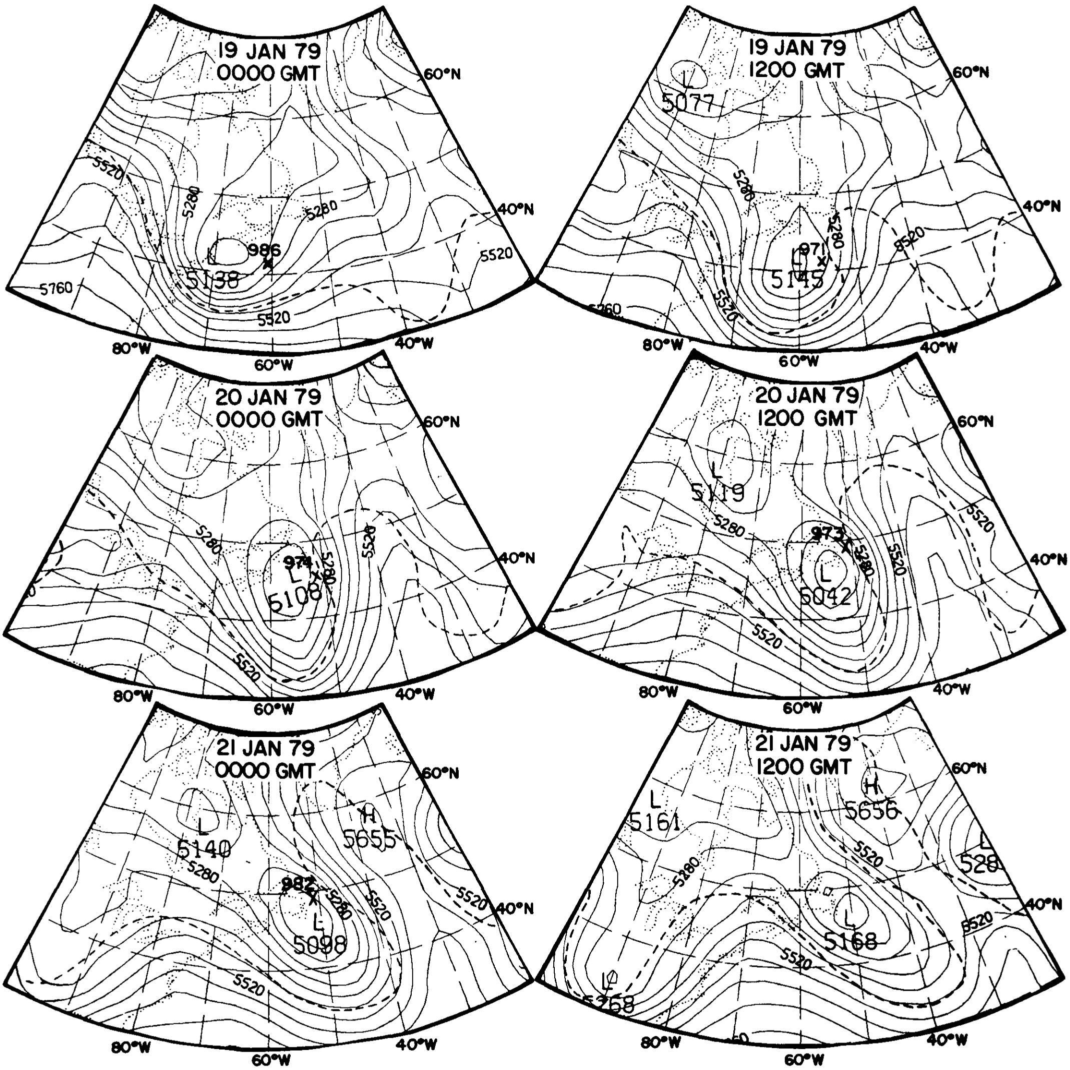

Fig. 3. As in Fig. 2 for the period from 00.00 GMT 19 January through 12.00 GMT 21 January 1979.

value at 12.00 GMT 19 January. By 00.00 GMT 20 January, the slow-moving ridge became stationary and began to build northward. Over the remaining 36 h displayed, the ridge continued to amplify. Accompanying this ridge amplification was strong warm air transport which gradually warmed the air at the northern extent of the ridge. In addition, strong height gradients progressed from south to east of the low upstream from the ridge. A warm core high at 500 mb first appeared on 00.00 GMT 21 January southeast of southern Greenland, followed 12 h later by the formation of a closed anticyclone over southern Greenland. This feature, which is quite distinct from another anticyclone that formed several days earlier south of Iceland, persisted in nearly the same location for the next week while diverting migrating cyclones to its west and south. Thus, it can be properly regarded as a blocking anticyclone event. A more detailed synoptic discussion of this case is presented in TS.

Table 1. *Time variation of AN and QG eddy kinetic energy (KE); units: 10^5 J m^{-2}*

	KE	
Date/time	AN	QG
17/12	14.1	16.8
18/00	13.6	16.9
18/12	12.0	15.0
19/00	12.5	14.9
19/12	12.8	14.4
20/00	13.7	14.5
20/12	14.7	16.1
21/00	16.0	15.9
21/12	16.5	16.1
AVE (17/12–21/12)	14.0	15.6
AVE (18/12–21/12)	14.0	15.3

Table 2. *Time variation of the AN and QG baroclinic conversion of eddy available potential energy to eddy kinetic energy (CE) and barotropic kinetic energy exchange between zonal and eddy flows (CK); units: W m^{-2}*

	CE		CK	
Date/Time	AN	QG	AN	QG
17/12	+4.5	+7.6	−10.1	−17.7
18/00	+1.8	+4.4	−10.6	−16.7
18/12	+4.3	+5.9	−7.9	−12.7
19/00	+7.7	+6.3	−6.8	−7.2
19/12	+8.4	+8.2	−4.4	−7.4
20/00	+7.9	+7.9	−4.3	−2.3
20/12	+6.4	+6.8	−5.0	−5.6
21/00	+7.1	+6.0	−5.7	−8.1
21/12	+8.3	+5.8	−4.0	−7.5
AVE (17/12–21/12)	6.3	6.5	−6.5	−9.5
AVE (18/12–21/12)	7.2	6.7	−5.4	−7.2

4. Results

4.1. Energetics diagnoses

Recall that the energetics analysis is restricted to diagnoses of vertically-integrated, area-averaged eddy kinetic energy content (KE) and baroclinic (CE) and barotropic (CK) eddy kinetic energy exchanges. The region chosen for the area average, which covers the blocking high and its upstream cyclone, is depicted in Fig. 1. Table 1 depicts the time variation of KE in the AN and QG form during the development of the block. Note that the QG KE values were consistently larger than the analyzed, indicating that the QG calculations generally overestimated the wind speeds. Differences are also seen in the time evolution of the sets of values. The AN KE values decreased initially but then began to increase at 12.00 GMT 18 January, the time that rapid cyclogenesis began. KE increased throughout the remaining period as the cyclone matured and the block developed. The rate of increase was greatest during the 24-h period from 00.00 GMT 20 January, when the ridge became stationary, to 00.00 GMT 21 January, when the closed high first appeared. In the QG KE results, KE increases did not begin until 24 h after the AN values and were not particularly well-correlated with any of the key synoptic events.

The time variations of the AN and QG form of CE and CK are given in Table 2. For both terms a positive (negative) value indicates a source (sink) of KE. Both the AN and QG forms of CK were negative throughout the entire period of investigation, although NQG processes resulted in a weaker KE sink (AN CK values less than QG CK). Thus, the eddies converted kinetic energy to the zonal flow, indicating that the eddies were barotropically stable. This result is consistent with that of Chen and Shukla (1983), who examined the energetics of a 1976–1977 winter block and also found that the eddies were barotropically stable. On the other hand, the CE results show that the eddies were baroclinically unstable. The conversion of eddy potential to kinetic energy was most vigorous during the explosive development phase of the cyclone and the amplification of the blocking ridge in both results. However, the AN form of CE was comparable or greater than the QG form. The signs of both CE and CK are in agreement with Kung and Tanaka's (1983) global energetics analysis during SOP-1 and Holopaninen and Fortelius' (1987) study of a blocking case using time mean/eddy analyses.

Viewing the sets of tabular results together we see that 12.00 GMT 18 January is significant when evaluating the impact of NQG processes. During the period of explosive cyclogenesis and subsequent block development, AN KE systematically increased. Similar increases in QG KE

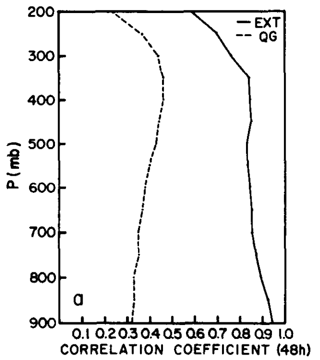

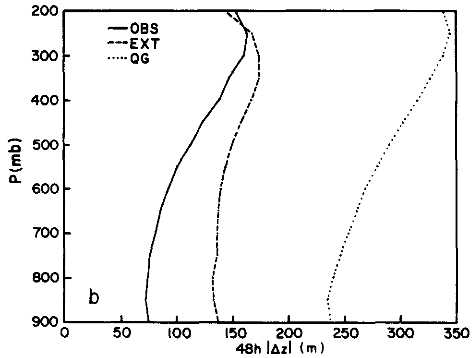

Fig. 4. (a) Vertical profiles of correlation coefficients comparing observed with EXT and observed with QG height tendencies for the 48-h period 12.00 GMT 19 January through 12.00 GMT 21 January. (b) Vertical profiles of 48 h area-mean absolute observed, QG, and EXT height tendencies.

are seen only after cyclone development ended. In addition this same period was marked by general increases in AN CE and little overall change in the corresponding QG quantity. As a result the AN baroclinic energy source exceeded the AN barotropic energy sink, while QG CE was slightly less that QG CK. From this we conclude that NQG processes systematically strengthened the eddy circulations associated with the developing block and preceding cyclone and that a portion of this increase resulted from an enhanced baroclinic energy source and a reduced barotropic energy sink.

4.2. Height tendency diagnoses

Before considering the NQG contributions, we first compare EXT and QG tendencies with observed height changes, the latter determined as the simple difference between the height fields at the beginning and end of a period. Adopting the philosophy of Tsou et al. (1987) comparisons are made for 48-h height changes, with those obtained from the tendency equations being obtained by integration over the 48 h period using the trapezoidal rule with 12-h subintervals. To compare the performance of QG and EXT equations during the development of the block, the 48-h period from 12.00 GMT 19 January to 12.00 GMT 21 January, spanning the time from 12 h before the ridge became stationary to the time of block formation was selected. Results are displayed in Fig. 4. Fig. 4a shows profiles of correlation coefficient between the 48 h observed and the two model height tendencies. The EXT height tendencies correlated well with the observed height tendency fields, while the QG patterns compared less favorably. Fig. 4b shows vertical profiles of 48-h area-mean absolute tendencies derived from the two models and observed calculations. Clearly, both models have overestimated the height tendencies. However, the overestimate by the QG model was much more serious than the EXT model at all levels. Thus, NQG processes oppose the QG processes, resulting in a reduction of height tendencies during the 48-h block development period.

The comparisons presented in Fig. 4 allow us to regard the EXT estimates as the superior of the two models and to attribute any differences between the EXT and QG model calculations to deficiencies in the QG model. To provide an overall comparison of EXT and QG tendencies, two comparative statistics are shown in Fig. 5. Displayed for each map time are the correlation coefficient between QG and EXT height tendencies (5a) and the ratio of QG to EXT area mean absolute height tendencies (5b), with both statistics presented for the total combined and each individual forcing process at 500 mb. Height tendency patterns due to the total forcing calculated from the two models did not correlate well (Fig. 5a), with the smallest correlation occurring during the 24-h period from 00.00 GMT 20 January, when the ridge became stationary, to 00.00 GMT 21 January, when the closed high first appeared. Thus, NQG processes made their most important contributions to the total height change pattern during the block development.

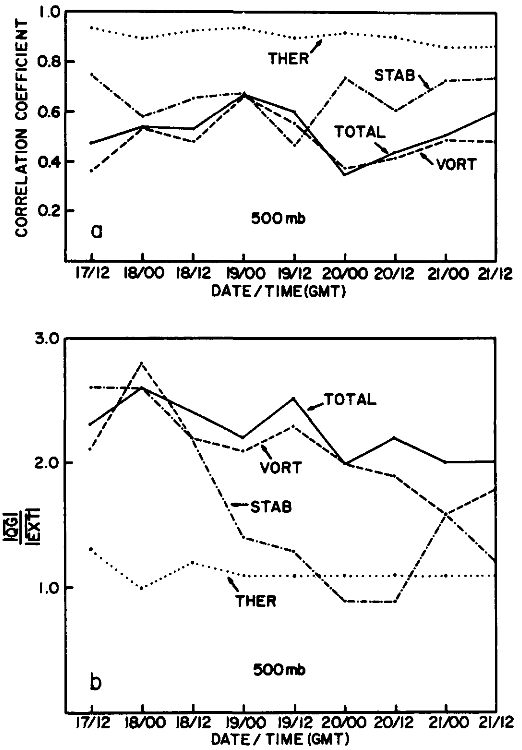

Fig. 5. (a) Time variation of correlation coefficients comparing EXT and QG height tendency fields for the total and individual forcing terms at 500 mb. (b) Time variation of the ratio of QG to EXT area mean absolute height tendencies for the total and individual forcing terms at 500 mb. All dates are for January 1979.

The corresponding ratio values (Fig. 5b) confirm that the QG tendencies were consistently a factor of two larger than the EXT.

Considering the same statistics for each forcing term, it is obvious that the differential thermal advection (THER) was very similar in both the QG and EXT height tendency calculations. This is similar to Mudrick's (1982) model results, which showed QG and primitive equation model horizontal heat fluxes to be similar. However, the height tendency patterns due to vorticity advection (VORT) and stability advection (STAB) calculated from the two models were poorly correlated. In addition, height tendencies due to both QG advections were significantly overestimated. Although the overestimate during the second half period was less serious than the first half period, NQG vorticity and stability advections still made important contributions to both the pattern and magnitude of the height tendencies associated with the developing block and the upstream cyclone.

To further compare the height tendencies, horizontal distributions of QG and EXT height tendencies attributed to the total combined forcing and each individual forcing term at 500 mb are shown in Figs. 6–7 and 8–9, respectively. In general, prior to 00.00 GMT 20 January the gross features of the height tendency fields (not shown) were similarly represented by the QG and EXT models. However, as expected from the previous results, the magnitude of the QG maxima were much larger than the EXT. The height tendency fields due to the individual forcing terms show that the larger QG calculations were mainly contributed by the vorticity advection. In Holton's (1979, pp. 132–135) physical interpretation of the influence of each forcing term, the QG vorticity maximum and minimum coincide with the trough and ridge in the height field, since the height field was assumed to consist of a single sine wave only. Thus, in his analysis the QG vorticity advection could not occur along the troughs and ridges. This means that the QG vorticity advection could only contribute to the propagation of a wave, while the intensity of a wave is controlled by the differential thermal advection. Although this simplified physical interpretation can be applied to a single-wave system, it is less applicable to the real atmosphere, where the wave systems are much more complicated. In the present study, vorticity advection was the primary forcing term for both the propagation and intensification of the ridge of interest. The differential thermal advection, which was quite comparable in both the QG and EXT height tendency calculations, played a secondary role.

The static stability advection played the same role in both the QG and extended height tendency fields. Its main effect was to offset the propagation and amplification of the ridge contributed by the vorticity and differential thickness advection. The braking effect of static stability advection was smaller for the QG than for the EXT height changes in the vicinity of the ridge and the upstream trough. Although less important than the vorticity advection, this smaller braking effect seen in the QG calculation also

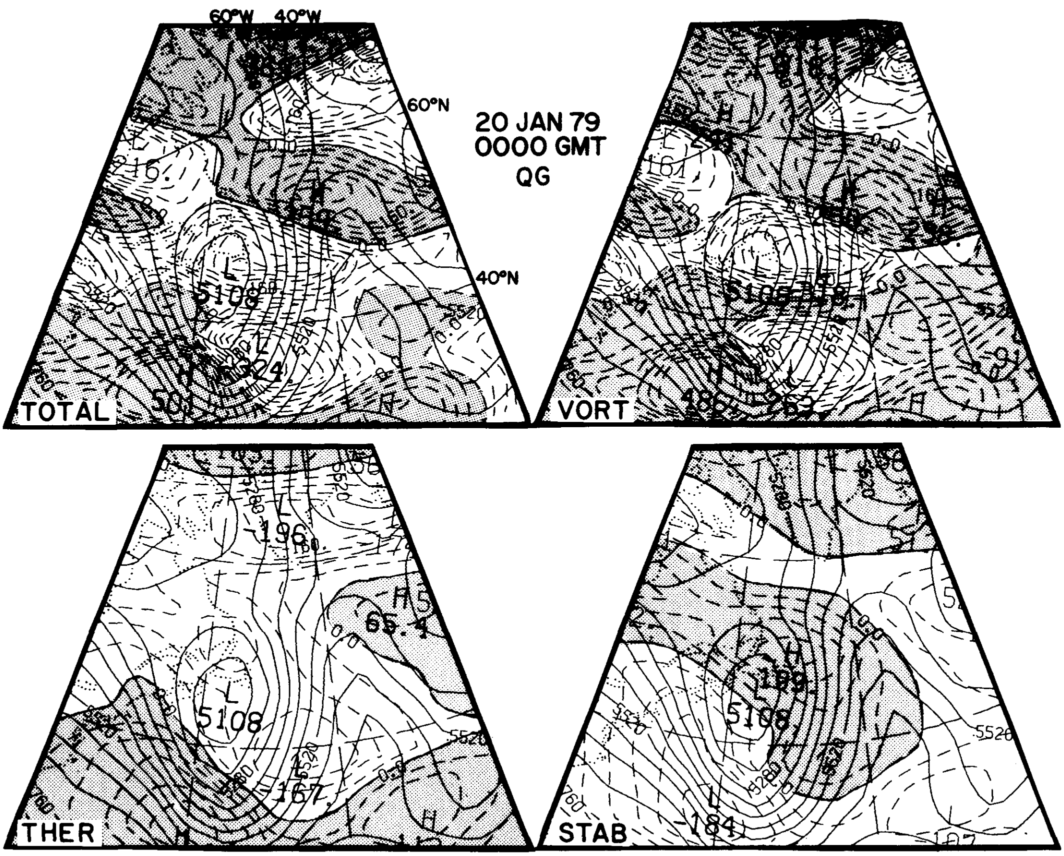

Fig. 6. Analyzed heights (solid, *m*) with QG height changes (dashed, *m* [12 h^{-1}]) attributed to the total and individual forcing terms (A, B, and C in [4]) for 00.00 GMT 20 January. Height rise areas shaded.

contributed to the larger total QG height tendency fields.

At 00.00 GMT 20 January 1979, when the ridge became stationary, the QG estimates were again larger than the EXT almost everywhere (compare Figs. 6 and 8). However, in the crucial area around the stationary ridge, QG height rises were less that the EXT. Comparing the QG and EXT height tendencies due to the individual forcing, it is obvious that the smaller QG values were primarily due to the weaker QG vorticity advection over the northern extent of the ridge. Again, the QG differential thermal advection successfully captured the height change in the vicinity of the ridge, with the height rise maximum located on the east side of the ridge. The main effect of differential thermal advection was to propagate the ridge eastward. However, this effect was opposed by the height falls due to the static stability advection.

Before comparing height tendency fields at 00.00 GMT 21 January, when the closed high first appeared, it is of interest to investigate the QG height tendency fields 12 h earlier. Fig. 10 shows for both the EXT and QG models the total height tendencies and those due to vorticity advection at 12.00 GMT 20 January. Height tendencies due to differential thermal and σ advection are not displayed because they were similar in both the EXT and QG results. As seen 12 h earlier, the QG model height rises were smaller than the EXT over the northern extent of the ridge. However, of particular importance is the fact, in contrast with the EXT estimates, that

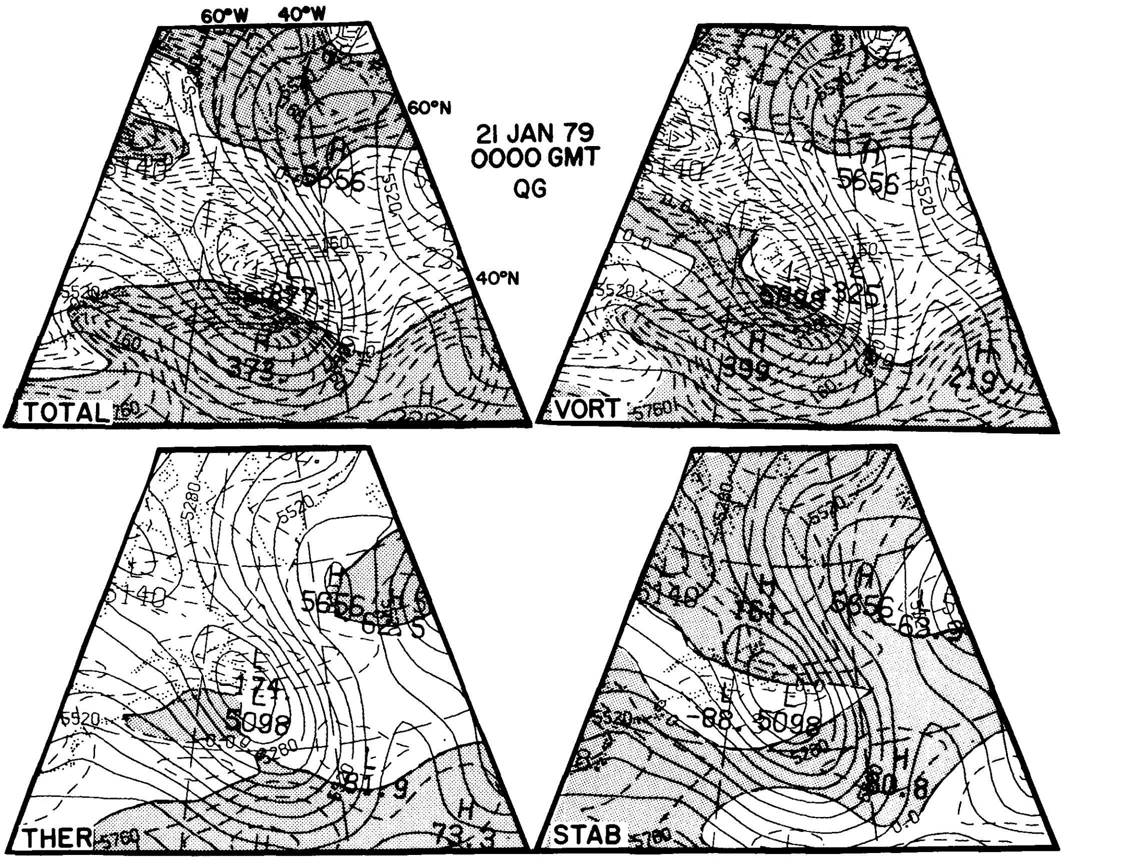

Fig. 7. As in Fig. 6 for 00.00 GMT 21 January.

no QG height rise maximum was located on the northern extent of the ridge. This pattern was mainly produced by the QG vorticity advection, which yielded much smaller height rises than the EXT model in the ridge at this time. In fact, considering that QG height rises were also smaller 12 h earlier, it is quite possible that the QG model would be unable to form the closed high analyzed at the following map time. This would imply that the NQG vorticity advection played a crucial role in the development of the anticyclone.

By 00.00 GMT 21 January, the QG model height rises were again larger than the EXT model values in the vicinity of the high (compare Figs. 7 and 9). This dramatic change from the underestimate 12 h earlier might lead us to believe that the gross features of the block, first observed 12 h later, were well-described by the QG model. However, if, as suggested above, the QG model were unable to form the initial closed high, then even strong height rises at this time might not have been sufficient to force further block development. In other words, the QG model might not produce a block at all. This in fact was the case in the numerical model study reported by Bengtsson (1981). Studying a block that formed just prior to the one of interest in this study, he found that the high resolution ECMWF model successfully predicted the block, while a QG model did not.

To investigate the reasons that the QG vorticity advection forced weaker height changes as the ridge became stationary, the AN and QG relative vorticity fields on 20 January are shown in Figs. 11–12. Recall that the AN fields were

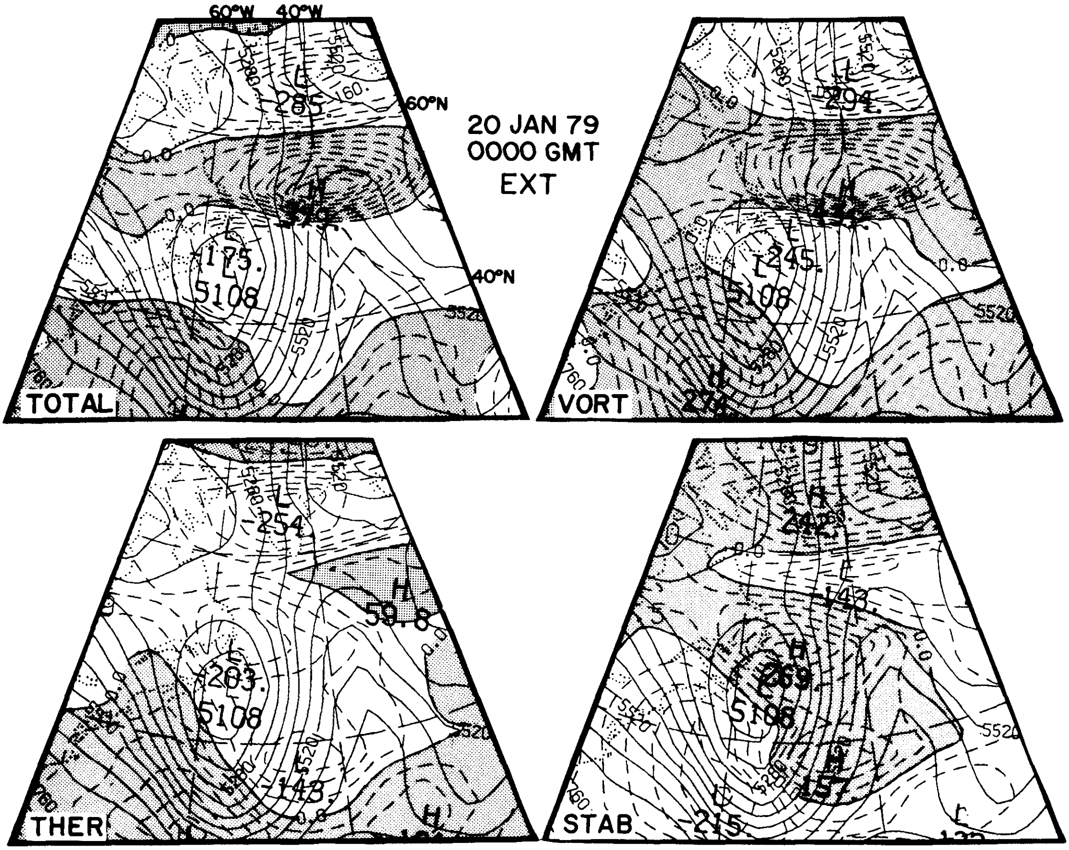

Fig. 8. As in Fig. 6 with EXT height changes from (3) for 00.00 GMT 20 January.

used in the EXT tendency calculations. To highlight areas with relatively strong anticyclonic vorticity, regions where the relative vorticities were less than -2×10^{-5} s^{-1} are shaded. At 00.00 GMT 20 January (Fig. 11), a broad shaded area is seen in the vicinity of the ridge. Both the AN and QG anticyclonic vorticity maxima were greatly increased over the previous times (not shown), reflecting the observed intensification of the ridge; and the magnitude of the QG anticyclonic vorticity maximum was larger than that of the analyzed. Even so, the height rises forced by vorticity advection in the vicinity of the ridge were smaller in the QG model than in the EXT. This can be explained by examining the relationship between the vorticity and wind fields. Figs. 11 and 12 depict wind vectors superimposed on the height and vorticity fields. In general, at 00.00 GMT the AN winds and vorticity gradients were somewhat greater than the QG in the region of the height rise maximum. At 12.00 GMT 20 January the differences between the AN and QG winds were even greater. Thus, both stronger winds and enhanced vorticity gradients in the AN fields contributed to larger negative vorticity advection and significantly greater EXT height rises at the northern extent of the ridge.

5. Summary

The purpose of this study was to examine the impact of non-quasigeostrophic (NQG) processes during the development of a blocking anticyclone and a precursor, upstream intense cyclone. To

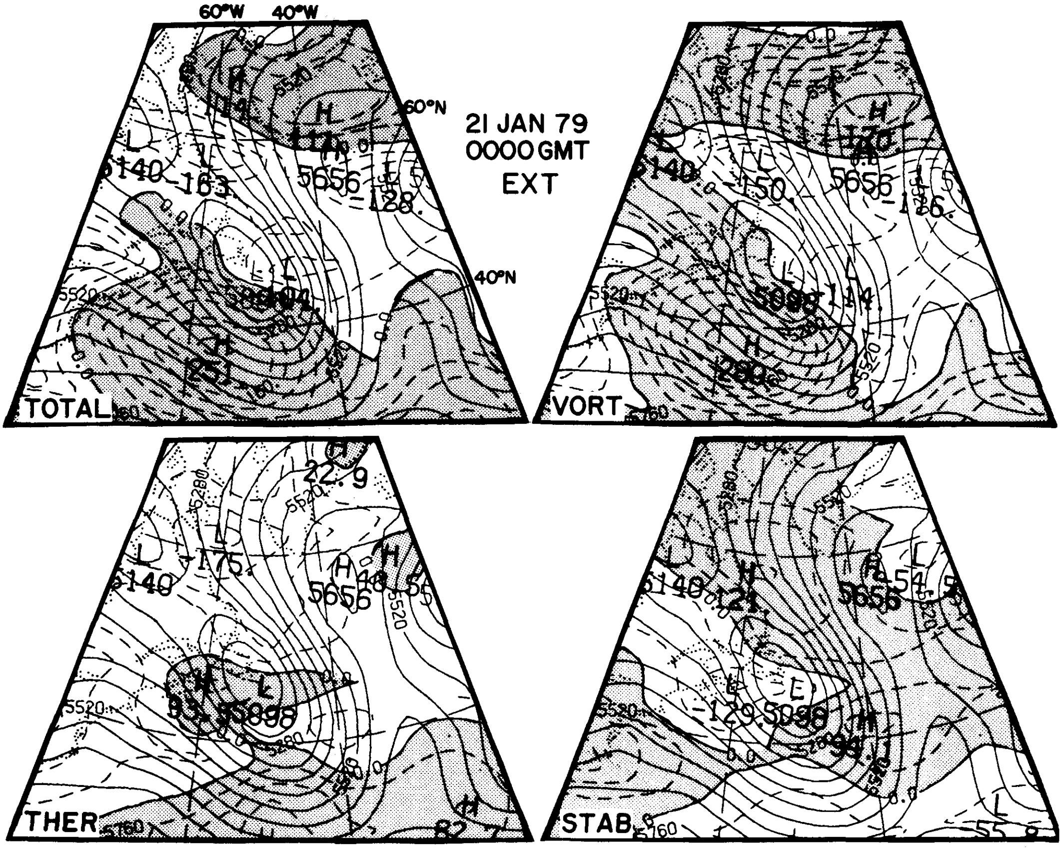

Fig. 9. As in Fig. 8 for 00.00 GMT 21 January.

accomplish this objective, energy quantities calculated from quasigeostrophic (QG) and analyzed (AN) data and height tendencies represented by the QG and extended (EXT) form of the height tendency equation were compared. The data used were SOP-1 FGGE III-b analyses obtained from GLA. The energetics results show that both the magnitude and the time variation of the AN and QG eddy kinetic energies (KE) differed. The former, which was smaller than the latter at all but the last two map times, increased systematically as the upstream cyclone and subsequent block developed; while the latter did not increase until 24 h after rapid cyclone development commenced. In both the QG and AN fields KE was maintained by baroclinic energy conversion and then lost barotropically to the zonal flow. However, more KE was baroclinically produced and less was barotropically lost in the AN flow than in the QG during the development of the block and its precursor cyclone. Thus, NQG processes strengthened the intensity of the eddy circulations during this period by enhancing the baroclinic energy source while reducing the barotropic energy sink.

The height tendency results indicate that the QG model, which compared less favorably to the observed height changes than did the EXT model, forced larger height changes than the EXT model everywhere prior to the time that the ridge became stationary. These larger QG values were caused primarily by larger QG vorticity advections. However, as the ridge became stationary, the QG model forced much smaller

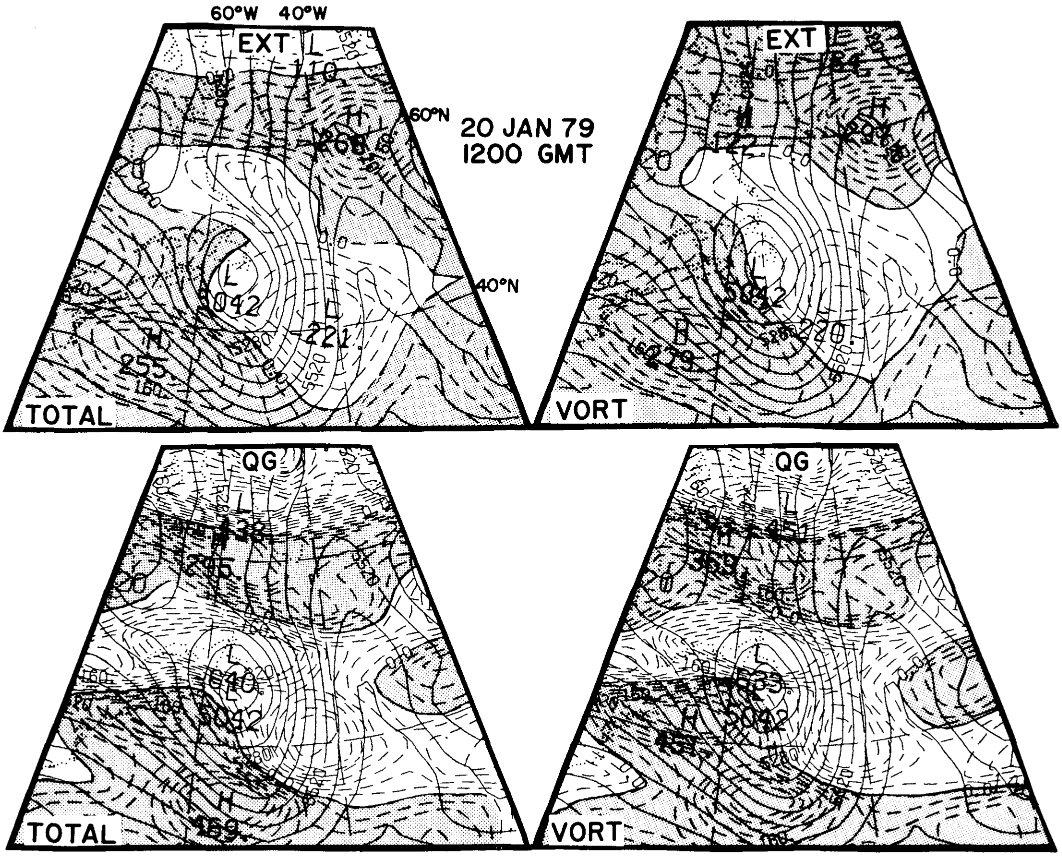

Fig. 10. Analyzed heights (solid, *m*) with EXT (top) and QG (bottom) height changes (dashed, *m* [12 h^{-1}]) attributed to the total forcing and the vorticity advection term for 12.00 GMT 20 January.

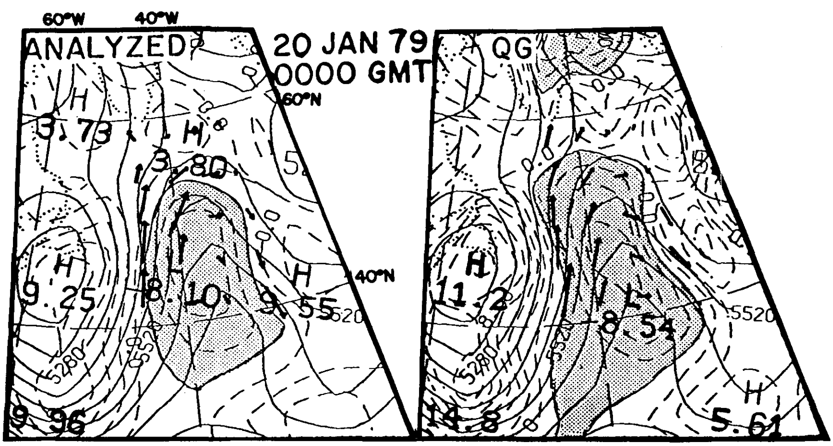

Fig. 11. Analyzed heights (both panels, solid, *m*) and vorticity fields (AN on left and QG on right, dashed, 10^{-5} s^{-1}) for 00.00 GMT 20 January. Shaded areas encompass regions of vorticity less than -2×10^{-5} s^{-1}. Heavy arrows represent wind vectors at selected grid points (AN on left, QG on right).

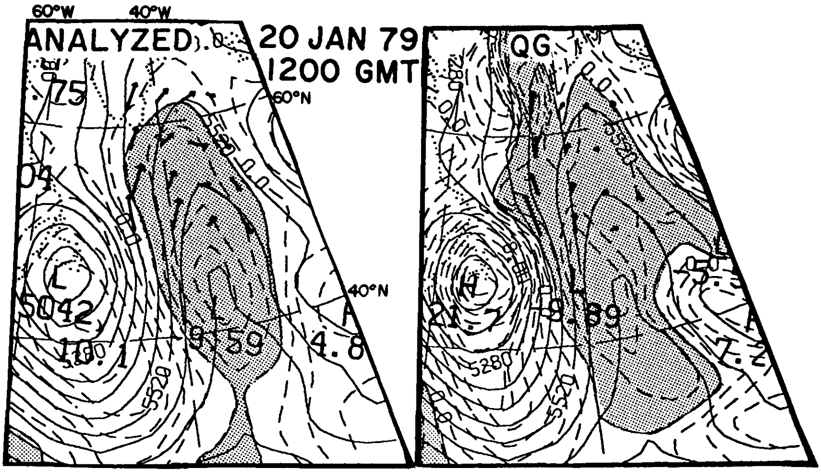

Fig. 12. As in Fig. 11 for 12.00 GMT 20 January.

height rises than the EXT model at the northern extent of the ridge. This was caused by smaller QG vorticity advection due to weaker winds and vorticity gradients. This implies that NQG vorticity advection played an important role during the growth of the ridge. In fact, QG processes alone might not have been able to form the block of interest, in agreement with the results of Bengtsson (1981).

6. Acknowledgements

The authors wish to thank Helen Henry for typing the manuscript and Richard Knabb for preparing the figures. Thanks are also extended to the referees for their very helpful criticisms. This work was supported by the National Aeronautics and Space Administration under Contract NAS 834009 and Grant NAG8-764.

REFERENCES

Baker, W. E. 1983. Objective analysis and assimilation of observational data from FGGE. *Mon. Wea. Rev. 111*, 328–342.

Bengtsson, L. 1981. Numerical prediction of atmospheric blocking—A case study. *Tellus 33*, 19–42.

Chen, T.-C. and Shukla, J. 1983. Diagnostic analysis and spectral energetics of a blocking event in the GLAS climate model simulation. *Mon. Wea. Rev. 111*, 3–22.

Colucci, S. J. 1985. Explosive cyclogenesis and large-scale circulation changes: Implications for atmospheric blocking. *J. Atmos. Sci. 42*, 2701–2717.

Colucci, S. J. 1987. Comparative diagnosis of blocking versus nonblocking planetary-scale circulation changes during synoptic-scale cyclogenesis. *J. Atmos. Sci. 44*, 124–139.

Cressman, G. 1959. An operational objective analysis system. *Mon. Wea. Rev. 87*, 367–374.

Gall, R. 1977. Some non-quasigeostrophic effects in linear baroclinic waves. *Mon. Wea. Rev. 105*, 1039–1051.

Green, J. S. A. 1977. The weather during July 1976: Some dynamic considerations of the drought. *Weather 32*, 120–126.

Hansen, A. R. and Chen, T.-C. 1982. A spectral energetics analysis of atmospheric blocking. *Mon. Wea. Rev. 110*, 1146–1165.

Holopainen, E. and Fortelius, C. 1987. High frequency transient eddies and blocking. *J. Atmos. Sci. 44*, 1632–1645.

Holton, J. T. 1979. *An introduction to dynamic meteoroloqy*, 2nd edition, Academic Press, 391 pp.

Kung, E. C. and Tanaka, H. 1983. Energetics analysis of the global circulation during the special observation period of FGGE. *J. Atmos. Sci. 40*, 2575–2592.

Mudrick, S. E. 1982. A study of adequacy of quasigeostrophic dynamics for modeling the effect of cyclone waves on the large scale flow. *J. Atmos. Sci. 39*, 2414–2430.

Mullen, S. L. 1987. Transient eddy forcing of blocking flow. *J. Atmos. Sci. 44*, 3–22.

Phillips, N. A. 1963. Geostrophic motion. *Rev. Geophy. 1*, 123–176.

Robertson, F. R. and Smith, P. J. 1983. The impact of model moist processes on the energetics of extratropical cyclones. *Mon. Wea. Rev. 111*, 723–744.

Smith, P. J. and Tsou, C.-H. 1988. Static stability variations during the development of an intense extratropical cyclone. *Mon. Wea. Rev. 116*, 1245–1250.

Tsou, C.-H., Smith, P. J. and Pauley, P. M. 1987. A comparison of adiabatic and diabatic forcing in an intense extratropical cyclone system. *Mon. Wea. Rev. 115*, 763–786.

Tsou, C.-H. and Smith, P. J. 1990. The role of synoptic/planetary-scale interactions during the development of a blocking anticyclone. *Tellus 42A*, 174–193.